# Half-quantized Hall effect at the parity-invariant Fermi surface

Jin-Yu Zou, Rui Chen, Bo Fu ⬡,* Huan-Wen Wang ⬡, Zi-Ang Hu, and Shun-Qing Shen†

*Department of Physics, The University of Hong Kong, Pokfulam Road, Hong Kong 999077, China*

Condensed matter realization of a single Dirac cone of fermions in two dimensions is a long-standing issue. Here we report the discovery of a single gapless Dirac cone of half-quantized Hall conductance in a magnetically doped topological insulator heterostructure. It demonstrates that the Hall conductance is half-quantized in the unit $e^2/h$ when the parity symmetry is preserved near the Fermi surface. The gapless Dirac point is stable and protected by the local parity symmetry and the topologically nontrivial band structure of the topological insulator. The one-half Hall conductance observed in a recent experiment [M. Mogi *et al.*, Nat. Phys. **18**, 390 (2022)] is attributed to the existence of the gapless Dirac cone and the parity invariance of the Fermi surface. The results suggest a condensed matter realization of a topological phase with a one-half topological invariant.

## I. INTRODUCTION

The search for a single gapless Dirac cone of fermions is a long-standing issue in condensed matter physics [1–3]. In quantum field theory, an ideal massless two-dimensional Dirac fermion coupled to a U(1) gauge field gives rise to the parity anomaly, characterized by a half-quantized Hall (HQH) conductance [4–8]. Lattice regularization of a single gapless Dirac cone on a lattice is not realizable if the parity symmetry is preserved according to the fermion doubling theorem [9]. One possible scheme is Wilson fermions, which possess linear dispersion near the energy crossing point, but break the time-reversal symmetry at higher energy [10,11]. The proposal for the condensed matter realization of parity anomaly dates back to the 1980s [12–14]. In his seminal paper [14], Haldane proposed that when the band gap of one valley on a honeycomb lattice is finely tuned to be closed while another one remains open, a single flavor of massless Dirac fermion with parity anomaly can be realized. In graphene, the parity anomaly with HQH effect is masked in view of the fourfold degeneracy from the spin and valley in the system [15]. Due to the presence of the parity symmetry, the paired Dirac cones give rise to contributions to the anomaly terms with opposite signs and thus exhibit no anomaly as a whole [16,17]. A three-dimensional topological insulator hosts a single Dirac cone of fermions on its surface [18–21]. It provides a possible platform to observe the HQH conductance and many attempts have been made in that direction [22–29]. Recently, the observation of the HQH conductance in transport at zero magnetic field was reported as a signature of the parity anomaly in a semi-magnetic topological insulator heterostructure [30]. The paired gapless Dirac cones in a topological insulator thin film are located separately on the top and bottom surfaces. The local time-reversal symmetry breaking on one surface by magnetic doping may open an energy gap for the Dirac surface fermions while the Dirac fermions remain gapless on

the other surface. Existing theories suggest that the massive Dirac fermions in the continuum give rise to HQH conductance [22,23]. However, it is known that all the independent bands on a two-dimensional finite Brillouin zone just have an integer Chern number [31,32]. Thus massive Dirac fermions with an HQH conductance cannot exist on a lattice. Contrarily, the gapless Wilson fermions in two dimensions have an HQH conductance and form a quantum anomalous semimetal when the valence bands are fully filled [33,34]. Thus the semi-magnetic topological insulator becomes a potential candidate to realize a single gapless Dirac cone in condensed matter.

In this work, we report the discovery of the gapless Dirac cone of HQH conductance in a semi-magnetic topological insulator heterostructure. The main results are summarized in Fig. 1. The gapless Dirac cone always has the HQH conductance in the units of $e^2/h$ when the parity symmetry is preserved at the Fermi surface. The gapless Dirac point is protected by the local parity symmetry and the topologically nontrivial band structure of the topological insulator, although the parity symmetry was broken at high energy. The gapped Dirac cone has a nonzero Hall conductance, but becomes zero when the band is fully filled. So the massive Dirac fermions alone do not contribute an HQH conductance to the system. The system has a minimal longitudinal conductance and exhibits a flat plateau of the HQH conductance when the Fermi level sweeps the Dirac cone. The plateau is very robust against the disorders. We term the gapless Dirac cone as a parity anomalous semi-metal, a semi-metal with a half-quantized Hall conductance. The results suggest a condensed matter realization of the topological phase with a one-half topological invariant.

## II. BAND STRUCTURE OF A SEMI-MAGNETIC TOPOLOGICAL INSULATOR

A semi-magnetic topological insulator film consists of topological insulator $(Bi, Sb)_2Te_3$ and Cr-doped $(Bi, Sb)_2Te_3$ grown by molecular-beam epitaxy. $(Bi, Sb)_2Te_3$ is a topological insulator with an energy gap of about 0.3 eV and hosts a single Dirac cone of the surface electrons [35–37]. As
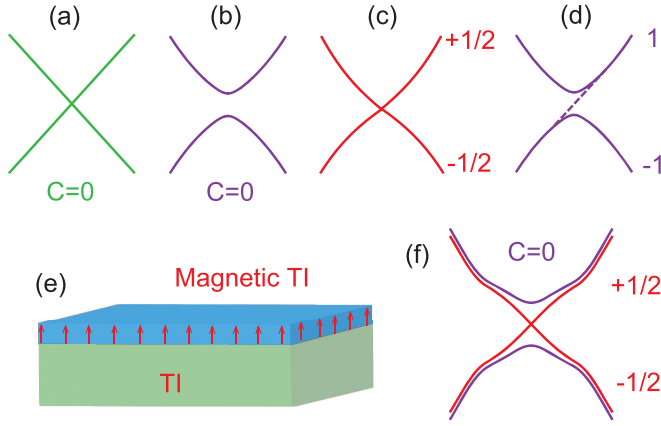
---

*fubo@hku.hk
†sshen@hku.hk

FIG. 1. Four types of two-dimensional Dirac fermions and parity anomalous semi-metal in a semi-magnetic topological insulator. (a) Ideal Dirac fermions with the Hall conductance $C = 0$ in the units of $\frac{e^2}{h}$, which cannot be realized on a lattice according to the fermion doubling theorem [9]. (b) Topologically trivial gapped Dirac fermion with $C = 0$. (c) The gapless Dirac fermions of linear dispersion at the Dirac point with $C = \pm 1/2$. (d) Topologically nontrivial gapped Dirac fermion with $C = \pm 1$, i.e., Chern insulator. (e) Schematic of a semi-magnetic topological insulator film. (f) Schematic of the band structure in a semi-magnetic topological insulator.
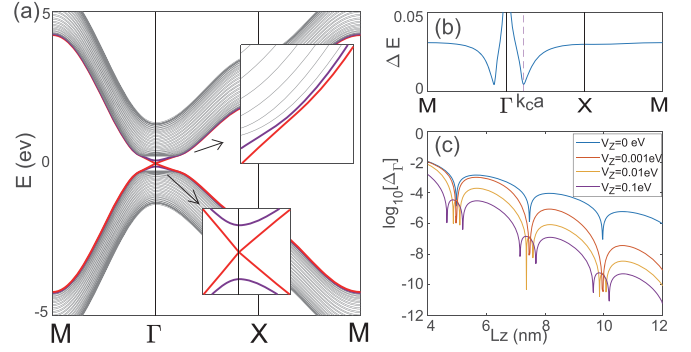


FIG. 2. The band structure of a semi-magnetic topological insulator. (a) The dispersions of well-separated gapless (red line) and gapped (violet line) Dirac cone in a topological insulator thin film of eight nonmagnetic layers plus two magnetic layers. Inset (1): The dispersions near the $\Gamma$ point. Inset (2): The antiband crossing point between the gapless and gapped Dirac cones. (b) The energy separation between the gapless and gapped Dirac cones. (c) The energy difference of the gapless Dirac cone at the $\Gamma$ point as a function of the thickness $L_z$ for several values of exchange interaction $V_z$ on the top layer. Model parameters: $\lambda_x = \lambda_y = \lambda_\parallel = 0.41$ eV, $\lambda_z = \lambda_\perp = 0.44$ eV and $t_x = t_y = t_\parallel = 0.566$ eV, $t_z = t_\perp = 0.40$ eV, and $m_0 = 0.28$ eV. $V_z = 0.1$ eV if no specific indication.

shown in Fig. 1(e), the magnetic element Cr was doped on the top surface. The exchange interaction between the magnetic ion and the surface electrons leads to nonzero magnetization and makes the top surface electrons open an energy gap [38–41]. The Fermi energy can be finely tuned by changing the ratio of Bi and Sb such that it locates within the band gap of the top surface Dirac cone. The topological nature of $(Bi, Sb)_2Te_3$ has been investigated extensively and can be well described by a tight-binding model for the electrons of $P_{z,\uparrow}$ and $P_{z,\downarrow}$ orbitals from (Bi, Sb) and Te atoms near the Fermi energy [25,35,42]

$$H_{TI} = \sum_i \Psi_i^\dagger \mathcal{M} \Psi_i + \sum_{i,\alpha=x,y,z} (\Psi_i^\dagger \mathcal{T}_\alpha \Psi_{i+\alpha} + \Psi_{i+\alpha}^\dagger \mathcal{T}_\alpha^\dagger \Psi_i), \quad (1)$$

where $\mathcal{M} = (m_0 - 2\sum_\alpha t_\alpha)\sigma_0\tau_z$, $\mathcal{T}_\alpha = t_\alpha\sigma_0\tau_z - i\frac{\lambda_\alpha}{2}\sigma_\alpha\tau_x$, $\Psi_i^\dagger$ and $\Psi_i$ are the four-component creation and annihilation operators at position $i$. The Pauli matrices $\sigma_\alpha$ and $\tau_\alpha$ act on the spin and orbital indices, respectively. All bands are doubly degenerate due to the coexistence of both time-reversal and inversion symmetries in the absence of magnetic doping. It can produce the linear dispersion of the surface states near the $\Gamma$ point in an open boundary condition [43]. The exchange interaction caused by Cr doping is given by a $V_{exch} = \sum_i \Psi_i^\dagger V(i)\sigma_z\tau_0\Psi_i$, which is only present on the top layers with the magnitude $V_z$. In experiments, the thickness of the Cr-doped $(Bi, Sb)_2Te_3$ is about 2 nm and $(Bi, Sb)_2Te_3$ layer is about 8 nm [30]. We take the periodic boundary condition in the $x$ and $y$ directions and the open boundary condition in the $z$ direction, the calculated dispersions are presented in Fig. 2(a). It is noted that there exist a gapless Dirac cone and a gapped Dirac cone within the bulk gap. The dispersions for the gapless Dirac cone cross at the $\Gamma$ point and are linear in $k$ around the crossing point. The gapped Dirac cone opens an energy gap of about $2V_z$. Numerical calculation shows that

the gapless and gapped states within the bulk band gap are mainly located on the bottom and top surfaces, respectively. We check the energy separation between the two bands along the high symmetric lines and find that the gapless Dirac cone and gapped Dirac cone are well separated. The dip at $k_c$ indicates that there exists a band mixture. Finite thickness of the film may cause a tiny gap at the $\Gamma$ point, which decays exponentially in the thickness approximately [44,45]. With increasing exchange interaction, the gap is further suppressed by several orders of magnitude to negligibly small [about $10^{-10}$ eV for a thickness $L_z = 10$ nm, see Fig. 2(c)]. It will be smeared out easily by temperature broadening (1K is about 0.086 meV) in experimental measurements.

## III. HALL CONDUCTANCE AND THE BERRY CURVATURE

Using the Kubo formula for the electric conductivity [46], we calculate the Hall conductance as a function of the chemical potential $\mu_F$ numerically based on the tight-binding model in Eq. (1) with a thickness $L_z = 10$ nm. A fairly flat plateau of $-\frac{e^2}{2h}$ appears within the band gap as shown in Fig. 3(a). To figure out the origin of the plateau of the Hall conductance, we first note that there exists a full band separation between the four lowest energy bands and the rest at all $k$. These four bands form well-separated band subspaces and the Hall conductance can be calculated for each band. We then only focus on the gapless and gapped Dirac cones denoted by the red and violet lines in Fig. 2(a). For the gapped Dirac cone, we have a nonzero Hall conductance as $\mu_F$ varies, which has its maximal about $0.4\frac{e^2}{h}$, but decays to zero quickly when the band is fully occupied. The maximal value may increase for a thicker film, but is always lower than $0.5\frac{e^2}{h}$. This is consistent with the fact that the Chern number of a well-defined band in a finite Brillouin zone is always an integer (including zero)
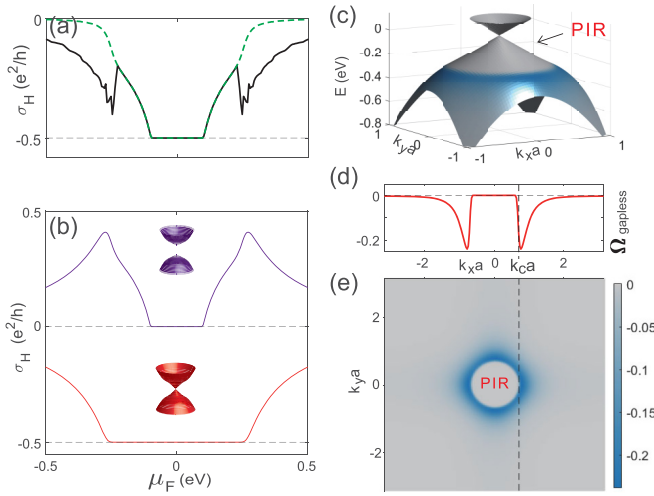
FIG. 3. (a) The Hall conductance as a function of the chemical potential $\mu_F$ for the thin film. The green dashed line is the combination of the Hall conductance of the gapless and gapped Dirac cones. (b) The Hall conductance of the gapless and gapped Dirac cones. (c) The gapless Dirac cone in a two-dimensional Brillouin zone. The color indicates the value of the Berry curvature of the states. (d) The Berry curvature of the gapless valence band as a function of $k_x$ ($k_y = 0$). (e) The Berry curvature and the parity-invariant regime (PIR) in the Brillouin zone.

[21,32]. This contrasts to the picture that the gapped Dirac cone leads to $0.5\frac{e^2}{h}$ of the Hall conductance [22,23,30]. For the gapless Dirac cone, the Hall conductance becomes $-0.5\frac{e^2}{h}$ within the bulk band gap, which is larger than the gap of the gapped Dirac cone. Thus the total Hall conductance within the bulk band gap is mainly contributed to by these two bands and the Hall conductance plateau is attributed to the gapless Dirac cone instead of the gapped Dirac cone.

To explore the topological nature of the gapless Dirac cone and its relation to the Hall conductance, we studied the Berry curvature of the gapless bands. In the Bloch states $|u_{n,\mathbf{k}}\rangle$, the Berry connection and the Berry curvature are defined as $\mathcal{A}_{n,\alpha}(\mathbf{k}) = i\langle u_{n,\mathbf{k}}|\partial_{k_\alpha} u_{n,\mathbf{k}}\rangle$ and $\Omega_z^n(\mathbf{k}) = \partial_{k_x}\mathcal{A}_{n,y}(\mathbf{k}) - \partial_{k_y}\mathcal{A}_{n,x}(\mathbf{k})$, respectively [32]. For the gapless Dirac cone, it is found that the Berry curvature $\Omega_z^n(\mathbf{k}) = 0$ within the regime of $k < k_c$ (parity-invariant regime which we will define in

the next section). Beyond the regime, it becomes negative and finally vanishes for a larger $k$. Combined with the band structure, the nonzero Berry curvature mainly originates from hybridization of the states from the top and bottom layers. It happens because the states are no longer localized near the surfaces and merge into the entire bulk in the regime of $k > k_c$. The conductance plateau appears when the chemical potential lies in the regime where the Berry curvature vanishes. For comparison, the Berry curvatures of the gapped bands are presented in Appendix A 4.

We would like to show that the Hall conductance is precisely quantized as a plateau by numerically calculating the precision of the half-quantized Hall conductance. The Berry curvature distribution in the parity-invariant regime is precisely zero, as shown in Fig. 4(a), in which the Berry curvature is negligibly tiny up to $10^{-10}$. Hence the Hall conductance will not change when the Fermi level sweep through this regime. Numerically, the deviation of the Hall conductance from one half $\sigma + \frac{e^2}{2h}$ is also zero. As we can see in Fig. 4(b), the precision is $10^{-6}$, and still can be enhanced if we continue increasing the density of the $k$ points.

## IV. ON THE PARITY-INVARIANT REGIME

Now we come to discuss the origin of the parity-invariant regime based on the tight-banding model in Eq. (1). For each wave vector $\mathbf{k}$, the Hamiltonian can be divided into two parts, $H_{TI}(\mathbf{k}) = H_{1d}(\mathbf{k}) + H_S(\mathbf{k})$. $H_{1d}$ is equivalent to a one-dimensional lattice model with an effective mass $m_0(k) = m_0 - 4t_\parallel(\sin^2\frac{k_xa}{2} + \sin^2\frac{k_ya}{2})$ [21],

$$H_{1d}(\mathbf{k}) = \sum_{i_z}\left(\Psi_{i_z,\mathbf{k}}^\dagger \mathcal{M}(\mathbf{k})\Psi_{i_z,\mathbf{k}} + \Psi_{i_z,\mathbf{k}}^\dagger \mathcal{T}_z\Psi_{i_z+1,\mathbf{k}} + \text{H.c.}\right),$$

$$(2)$$

with $\mathcal{M}(\mathbf{k}) = [m_0(k) - 2t_\perp]\sigma_0\tau_z$ and $H_S(\mathbf{k}) = \lambda_\parallel\sum_{i_z,\alpha=x,y}\Psi_{i_z,\mathbf{k}}^\dagger \sin(k_\alpha a)\sigma_\alpha\tau_x\Psi_{i_z,\mathbf{k}}$. For $m_0(k) > 0$, i.e., $k < k_c \simeq \sqrt{M/t_\parallel}/a$, $H_{1d}$ is topologically nontrivial. There exist a pair of zero energy modes at each side or near the top surface and bottom surface. Denote $\xi_s$ and $\chi_t$ the two eigenvectors of $\sigma_z$ and $\tau_y$ with eigenvalues $s = \pm 1$ and $t = \pm 1$. The zero energy modes are the eigenvectors $\xi_s \otimes \chi_t$ of the operator $\sigma_z\tau_y$ with the eigenvalue $S = st$. The spatial part of the two states of $S = 1$ ($s = t = 1$



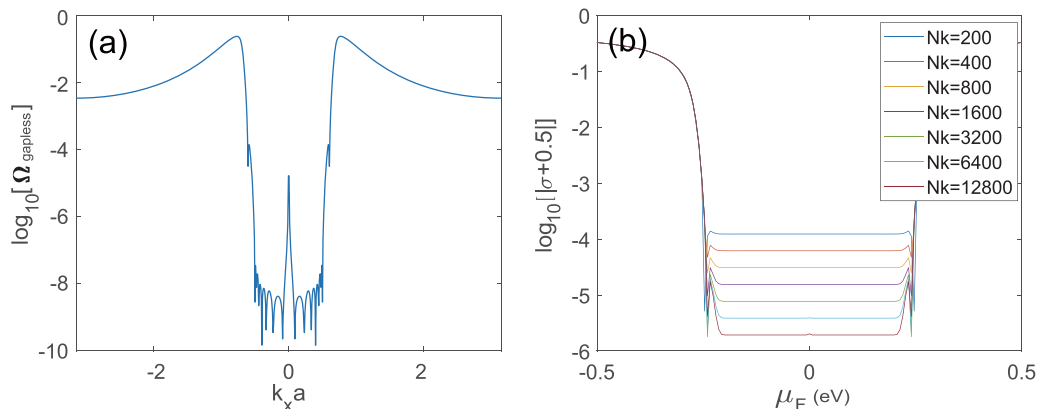FIG. 4. (a) The logarithm of the Berry curvature depending on $k_x(k_y = 0)$. (b) The logarithm of the deviation of the Hall conductance from one half. The $k$ points used in the calculation are $N_k \times N_k$ in the two-dimensional Brillouin zone.

and $s = t = -1$) are mainly located near the top surface and the two states of $S = -1$ are located near the top surface, and decay exponentially to its opposite side [21]. By mapping $H_S(\mathbf{k}) + V_{\text{exch}}$ into the basis of the four states, one obtains the effective Hamiltonian the gapless Dirac cone $H_b(k) = -\lambda_{\|}[\sin(k_x a)\sigma_y - \sin(k_y a)\sigma_x]$ which is mainly located at the bottom layer and the gapped Dirac cone $H_t(k) = +\lambda_{\|}[\sin(k_x a)\sigma_y - \sin(k_y a)\sigma_x] + V(k)\sigma_z$ which is at the top layer. $V(k)$ is given by the expectation of the exchange interaction $V_{\text{exch}}$, and varies with the wave vector, especially when $m_0(k) \to 0$ where the wave function of zero energy modes evolve to distribute broadly in space. In two dimensions, the parity symmetry is defined by $\mathcal{P}H(\mathbf{k})\mathcal{P}^{-1} = H(\hat{M}\mathbf{k})$, where $\mathcal{P} = i\sigma_y$ and $\hat{M}$ is the mirror operator in momentum space transforming $\mathbf{k} \to \hat{M}\mathbf{k} = (k_x, -k_y)$. Thus in the regime the gapless Dirac cone $\mathcal{P}H_b(\mathbf{k})\mathcal{P}^{-1} = H_b(\hat{M}\mathbf{k})$ respects the parity symmetry while the gapped Dirac cone $\mathcal{P}H_t(\mathbf{k})\mathcal{P}^{-1} \neq H_t(\hat{M}\mathbf{k})$ breaks the symmetry due to the presence of $V(k)$. Thus the nontrivial condition of $m_0(k) > 0$ defines a parity-invariant regime for the gapless Dirac cone. In addition to the local parity symmetry, $H_b$ also respects a space-time operator $I_{ST} = C_{2z}T$ where $C_{2z}$ is a twofold rotation about the $z$ axis and $T$ is local time-reversal operator. $I_{ST}^2 = +1$ imposes a further constraint on the Berry curvature, leading to $\Omega_z^n(\mathbf{k}) = 0$.

When $m_0(k) < 0$, $H_{1d}$ becomes topologically trivial. The zero energy modes evolve into the bulk states. Approximately, the states can be regarded as the ones confined in a quantum well of thickness $L_z$ with nonzero energy $\pm m_0(k)$. The states are no longer the eigenvectors of the operator $\sigma_z \tau_y$, and break the parity symmetry. Based on this picture, we obtain an effective four-band model

$$H_F = \lambda_{\|}(\sin k_x a\sigma_y - \sin k_y a\sigma_x)\gamma_z + V(k)\sigma_z(\gamma_z + 1) + H_\Delta^{\text{eff}},$$
$$(3)$$

where $H_\Delta^{\text{eff}} = f(k)m_0(k)\gamma_x$. A Fermi-Dirac-distribution-like factor or the sigmoid function $f(k) = [\exp(\frac{m_0(k)}{T^*}) + 1]^{-1}$ is introduced to describe the procedure that the surface states evolve into the bulk states with the wave vector moves out of the parity invariant regime. $\gamma_{x,z}$ are the Pauli matrices associated with the top and bottom surface states. A small $T^*$ is a model-specific parameter. The calculated results show that the model can reproduce the key features of the band structure. The Hall conductance as a function of $\mu_F$ is given by $\sigma_H^S = \frac{e^2}{2h}[S - \cos\phi_S(k_F^S)]$. The part of $S$ is mainly attributed to the term $H_\Delta^{\text{eff}}$ and the band splitting $V(k)$. For the gapless band of $S = -\text{sgn}(V_z)$, $\cos\phi_S(k_F^S) = 0$ in the parity-invariant regime and $\sigma_H^S = -\text{sgn}(V_z)\frac{e^2}{2h}$. For the gapped band of $S = \text{sgn}(V_z)$, $\cos\phi_S = \text{sgn}(V_z)$ for the full occupancy and $\sigma_H^S = 0$. They are in good agreement with the numerical results in Fig. 3(b). It is noted that the Hall conductance is only dependent on the sign of $V_z$. The details are referred to in Appendix A 3. In the regime of $k < k_c$, $H_\Delta^{\text{eff}} \sim 0$ and $V(k) \sim V_z$, the Hamiltonian is reduced to $H_F = \lambda_{\|}a(\mathbf{k} \times \boldsymbol{\sigma})_z\gamma_z + V_z\sigma_z(\gamma_z + 1)$ which is similar with Eq. (S16) of Ref. [30]. In that paper, the HQH conductance was attributed to the gapped Dirac cone due to the missing of the constant $S$ in the expression of $\sigma_H^S$, which is contrary to numerical results that the Chern number of the gapped Dirac cone is always 0. The inclusion of an ultravio-

let regulator $H_\Delta^{\text{eff}}$ guarantees a lattice regularization and also leads to different topologies of the band structure. It is worth pointing out that the anomalous Hall conductance should be determined by the entire occupied band in the entire Brillouin zone. Also in an ultra thin film, $H_\Delta^{\text{eff}}$ is not zero for $k < k_c$ due to the strong overlapping of the top and bottom surface states, which is beyond the scope of this work and needs further investigation.

## V. HALF-QUANTIZATION AND PARITY SYMMETRY

Now we present a relation between the half-quantization of the Hall conductance and the parity symmetry. In the Haldane model and the Wilson fermions, it was found that the Hall conductance is half-quantized when the chemical potential is located at the energy crossing point [14,33]. Here we prove that the Hall conductance is one half of an integer if the parity symmetry is respected at the Fermi level $\mu_F$. In two dimensions, the Berry connection for band $n$ is defined as $\mathcal{A}_n(\mathbf{k}) = -i\langle u_n(\mathbf{k})|\nabla_\mathbf{k}|u_n(\mathbf{k})\rangle$ and the Berry curvature is defined as $\Omega_{n,z}(\mathbf{k}) = -i\epsilon_{ij}\langle\partial_i u_n(\mathbf{k})|\partial_j u_n(\mathbf{k})\rangle$ where $|u_n(\mathbf{k})\rangle$ is the Bloch function of band $n$ with the eigenvalue as $\varepsilon_n(\mathbf{k})$, $\epsilon_{ij}$ is the Levi-Civita symbol, and indexes $i, j$ run only over $x, y$. The Hall conductance of the system equals the integral of the Berry curvature of the filled bands over the Brillouin zone (BZ) [32]

$$\sigma_{xy} = \frac{e^2}{2\pi h} \sum_n \int_{\text{BZ}} d^2\mathbf{k} \Omega_{n,z}(\mathbf{k})\theta(\varepsilon_{n,\mathbf{k}} - \mu_F).$$

Here we consider the situation that the Fermi energy $\mu_F$ intersects one or more bands and there are a certain number of completely filled bands (C.F.B.). For each partially filled band (P.F.B.), there will be one or more surfaces (Fermi surfaces) in momentum space separating the occupied levels from the unoccupied levels, which are closed loops in two dimensions. Using the Stokes theorem, for the partially filled bands the Berry curvature integral over the occupied states can be converted into the line integral with respect to the Fermi surfaces (FSs). Thus, we have

$$\sigma_{xy} = \frac{e^2}{h} \sum_{n\in\text{C.F.B.}} \int_{\text{BZ}} \frac{d^2\mathbf{k}}{2\pi} \Omega_{n,z}(\mathbf{k})$$
$$+ \frac{e^2}{h} \sum_{n\in\text{P.F.B.}} \oint_{\cup_a\text{FS}_a^n} \frac{d\mathbf{k}}{2\pi} \cdot \mathcal{A}_n(\mathbf{k}),\qquad(4)$$

where $\text{FS}_a^n$ is the $a$th Fermi surface of band $n$. According to the Thouless, Kohmoto, Nightingale, and den Nijs (TKNN) theorem, the first term in the bracket must be an integer for all the completely filled bands. The second term in the bracket is the sum of the Berry phases (divided by $2\pi$) along all the Fermi surfaces for the partially filled bands, which can take an arbitrary value without additional symmetry constraint.

Let us now prove that the line integral is equal to a half integer when the parity symmetry is respected at the Fermi surface $\text{FS}_a^n$. The Fermi surface with parity symmetry obeys

$$\mathcal{P}H(\mathbf{k})\mathcal{P}^{-1} = H(\hat{M}\mathbf{k}),$$

where $\mathcal{P}$ is the momentum-independent unitary operator that acts on the internal degrees of freedom, $\hat{M}$ is an operator in momentum space transforming $\mathbf{k} \to \hat{M}\mathbf{k}$. Since we have $\mathcal{P}H(\mathbf{k})|u_n(\mathbf{k})\rangle = \varepsilon_{n,\mathbf{k}}\mathcal{P}|u_n(\mathbf{k})\rangle = H(\hat{M}\mathbf{k})\mathcal{P}|u_n(\mathbf{k})\rangle$, the state

$\mathcal{P}|u_n(\mathbf{k})\rangle$ must be the eigenstate of $H(\hat{M}\mathbf{k})$ with eigenenergy as $\varepsilon_{n,\mathbf{k}}$. Thus, the presence of the parity symmetry at $FS_i^n$ connects two states which have the same energy

$$|u_n(\mathbf{k})\rangle = e^{i\theta_n(\mathbf{k})}\mathcal{P}^{\dagger}|u_n(\hat{M}\mathbf{k})\rangle,$$

where $e^{i\theta_n(\mathbf{k})}$ is a $U(1)$ phase. From which the Berry connection has the relation

$$\begin{aligned}
\mathcal{A}_{n,i}(\mathbf{k}) &= -i\langle u_n(\mathbf{k})|\partial_{k_i}|u_n(\mathbf{k})\rangle \\
&= -i\langle u_n(\hat{M}\mathbf{k})|\mathcal{P}e^{-i\theta_n(\mathbf{k})}\partial_{k_i}\left(e^{i\theta_n(\mathbf{k})}\mathcal{P}^{\dagger}|u_n(\hat{M}\mathbf{k})\rangle\right) \\
&= \partial_{k_i}\theta_n(\mathbf{k}) - i\sum_j J_{ij}\langle u_n(\hat{M}\mathbf{k})|\partial_{(\hat{M}\mathbf{k})_j}|u_n(\hat{M}\mathbf{k})\rangle \\
&= \partial_{k_i}\theta_n(\mathbf{k}) + \sum_j J_{ij}\mathcal{A}_{n,j}(\hat{M}\mathbf{k}),
\end{aligned}$$

where $J_{ij} = \partial(\hat{M}\mathbf{k})_j/\partial k_i$. Then we have

$$\oint_{FS_a^n}\frac{d\mathbf{k}}{2\pi}\cdot\mathcal{A}_n(\mathbf{k}) = \oint_{FS_a^n}\frac{d\mathbf{k}}{2\pi}\cdot\nabla_{\mathbf{k}}\theta_n(\mathbf{k})$$
$$+ \sum_{i,j}\oint_{FS_a^n}\frac{d\mathbf{k}_i}{2\pi}J_{ij}\mathcal{A}_{n,j}(\hat{M}\mathbf{k}). \quad (5)$$

On the left-hand side of Eq. (5), the line integral of the Berry connection is performed in an anticlockwise direction. Using $\sum_i d\mathbf{k}_i J_{ij} = d(\hat{M}\mathbf{k})_j$ and $\text{Det}J = -1$, the second term on the right-hand side of Eq. (5) transforms into $\oint_{FS_a^n}\frac{d\mathbf{k}}{2\pi}\cdot\mathcal{A}_n(\mathbf{k})$ where the line integral is performed in the clockwise direction, which leads to

$$2\times\oint_{FS_a^n}\frac{d\mathbf{k}}{2\pi}\cdot\mathcal{A}_n(\mathbf{k}) = \oint_{FS_a^n}\frac{d\mathbf{k}}{2\pi}\cdot\nabla_{\mathbf{k}}\theta_n(\mathbf{k}).$$

The $U(1)$ phase advances by $2\pi N$ with $N$ being an integer when $\mathbf{k}$ winds around a closed contour. The line integral of the Berry connection over the Fermi surface with parity symmetry is a half integer

$$\oint_{FS_a^n}\frac{d\mathbf{k}}{2\pi}\cdot\mathcal{A}_n(\mathbf{k}) = \frac{N}{2}. \quad (6)$$

With this result, we then return to the discussion of the Hall conductance [Eq. (4)]. If the Fermi surface consists of a single loop which is the case of the semimagnetic topological insulator and line integral of the Berry connection over the Fermi surface is quantized to $\pi$, the Hall conductance is half quantized. Here we want to emphasize that the half quantization in Eq. (6) is subjected to the symmetry of the Fermi surface. The extension to multiple loops is straightforward. The simplest example is graphene, which possesses the time-reversal symmetry and features a pair of massless Dirac cones. In the absence of magnetic field, we do not expect an anomalous Hall current to occur. This result can be understood from Eq. (6) that the two independent Fermi surfaces in graphene give rise to one half contributions to the Hall conductance which alternates in sign and exhibits no net effect. In a semi-magnetic topological insulator thin film, according to the proof, all the contributions from the massive Dirac cone are contained in the completely filled bands below the Fermi surface [the first term in the bracket of Eq. (4)], which only gives an integer-valued Hall conductance with the inclusion of the high-energy states as required by the TKNN theorem, and thereby is entirely irrelevant to determining the
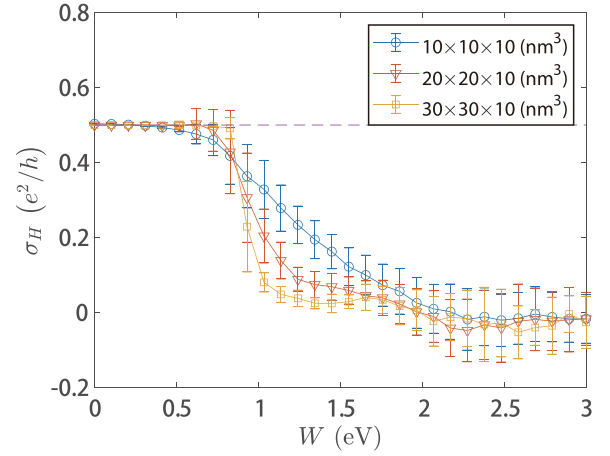


FIG. 5. The Hall conductance as a function of the strength of nonmagnetic disorders $U_i\sigma_0\tau_0$ for several lattice sizes $L_x\times L_y\times L_z$ for a fixed $L_z = 10$nm. The Fermi level $\mu_F = 0.01$ eV and the lattice spacing $a = 1$nm. Two hundred random configurations are adopted to average for each value.

half-quantization of the Hall conductance. We thus conclude the one-half Hall conductance is attributed to the existence of a single (i.e., undoubled) species of massless Dirac and the parity invariance of the Fermi surface.

## VI. DISORDERS AND ROBUSTNESS OF THE QUANTIZED HALL CONDUCTANCE

The robustness of the HQH conductance comes from two aspects. One is the local parity invariance for the gapless Dirac cone. The exchange interaction is only present at the top surface. The low-energy dispersion of the gapless Dirac cone is mainly located at the bottom layer and is less affected by the exchange interaction, although the part of the high energy is modified. The other aspect is that the presence of the surface states is mainly attributed to the $t$ topological insulator. It is known that the topology of its band structure is very robust against the disorders. If the strength of disorders is not strong enough to induce a topological phase transition, the gapless surface states are still present. In this way the Dirac point is very stable against the disorders before the phase transition occurs. To illustrate the robustness of the single Dirac cone in this quasi-two-dimensional system, we calculate the Hall conductance as a function of the strength of disorders. We follow the common practice in the study of Anderson localization to introduce disorder through random nonmagnetic on-site energy with a uniform distribution with $[-W/2, +W/2]$. We calculate the Hall conductance of a disordered square of size $L_x\times L_y\times L_z$ for a fixed thickness $L_z$ by means of the noncommutative Kubo formula [47]

$$\sigma_H = i2\pi\text{Tr}\{\mathbf{P}[-i[\mathbf{x},\mathbf{P}], -i[\mathbf{y},\mathbf{P}]]\}\frac{e^2}{h}, \quad (7)$$

with the periodic boundary conditions along the $x$ and $y$ directions. Here, $\mathbf{x}$ and $\mathbf{y}$ are the coordinate operators and $\text{Tr}\{\cdots\}$ is the trace over the occupied bands. $\mathbf{P}$ is the projector onto the occupied states of the system. Figure 5 shows the numerically calculated disorder-averaged Hall conductances as functions of the disorder strength. In the clean limit, the system exhibits the HQH conductance as expected. With increasing disorder

strength, the Hall conductance remains about $0.5\frac{e^2}{h}$ until the disorder strength $W$ exceeds about 0.83 eV. The critical disorder strength is much larger than the exchange interaction and also larger than the bulk energy gap of the topological insulator. Further increasing the disorder strength, the conductance drops quickly and the system is expected to be localized by disorders. Thus, the HQH conductance is robust against the disorder. This demonstrates explicitly that the gapless Dirac cone is quite stable against the disorders. It is further confirmed by calculating the self-energy in the self-consistent Born approximation based on the effective four-band model in Eq. (3) (see Appendix A 6).

The presence of impurities will cause the scattering between electron wave functions which leads to an energy-level repulsion effect [48]. The stability of the Dirac point is thus equivalent to examine the relative energy-level repulsion between the two states at the Dirac point from all other surface and bulk states. The scatterings between the two bottom surface states will not introduce Dirac mass renormalization due to the presence of the local time-reversal symmetry. The scatterings from the top surface states can also be neglected due to the fact that the two opposite surface states have exponentially small overlap. The magnetic doping on the top surface will cause an energy splitting $\sim V_z L_z^{\mathrm{mag}}/L_z$ for the two degenerate bulk states with $L_z^{\mathrm{mag}}$ as the thickness of the magnetic layers. For sufficiently small $L_z^{\mathrm{mag}}/L_z$, the energy level repulsion effect from two nearly degenerate bulk states will be canceled out. This picture is verified by a self-energy calculation in the self-consistent Born approximation based on the effective four-band model (Appendix A 6). Compared with the two-band model [49], the contributions to the Dirac mass renormalization from the gapped and gapless bands in the four-band model alternate in sign and cancel each other out at high energy. As a consequence, the Dirac point is still stable even in the presence of disorder due to the local time-reversal symmetry and the accompanying gapped bands.

## ACKNOWLEDGMENTS

## APPENDIX

### 1. Model Hamiltonian

Following the $k \cdot p$ model for the electrons of $P_z \uparrow$ and $P_z \downarrow$ orbitals from (Bi,Sb) and Te atoms of the topological insulator (Bi, Sb)$_2$Te$_3$ [35], we construct the tight-binding model on a cubic lattice in the basis of $\Psi = [P_z 1 \uparrow, P_z 1 \downarrow, P_z 2 \uparrow, P_z 2 \downarrow]^T$ [21],

$$H = \sum_i \Psi_i^\dagger \mathcal{M}_0(i)\Psi_i + \sum_{i,\alpha=x,y,z} (\Psi_i^\dagger \mathcal{T}_\alpha \Psi_{i+\alpha} + \Psi_{i+\alpha}^\dagger \mathcal{T}_\alpha^\dagger \Psi_i),$$

(A1)

where

$$\mathcal{M}_0(i) = \left(m_0 - 2\sum_\alpha t_\alpha\right)\sigma_0\tau_z + V(i)\sigma_z\tau_0;$$

$$\mathcal{T}_\alpha = t_\alpha \sigma_0 \tau_z - i\frac{\lambda_\alpha}{2}\sigma_\alpha\tau_x.$$

We take $\lambda_x = \lambda_y = \lambda_\parallel$, $\lambda_z = \lambda_\perp$, and $t_x = t_y = t_\parallel$, $t_z = t_\perp$. $V(i) = V_z$ is the exchange interaction in the Cr-doped layers and $V(i) = 0$ in the nondoped layers. For a thin film, we take a periodic boundary condition in the $x$ and $y$ directions and the open boundary condition in the $z$ direction. The model is reduced to

$$
\begin{aligned}
H_{\mathrm{Film}} = \sum_{i_z,\mathbf{k}} &\left(\Psi_{i_z,\mathbf{k}}^\dagger [m_0(\mathbf{k}) - 2t_\perp]\Psi_{i_z,\mathbf{k}}\right. \\
&+ \left.\Psi_{i_z,\mathbf{k}}^\dagger \mathcal{T}_z \Psi_{i_z+1,\mathbf{k}} + \mathrm{H.c.}\right) \\
&+ \sum_{i_z,\mathbf{k}} \Psi_{i_z,\mathbf{k}}^\dagger [H_P + V(i_z)\sigma_z\tau_0]\Psi_{i_z,\mathbf{k}},
\end{aligned}
$$

with

$$m_0(\mathbf{k}) = \left[m_0 - 4t_\parallel\left(\sin^2\frac{k_x a}{2} + \sin^2\frac{k_y a}{2}\right)\right]\sigma_0\tau_z;$$

$$H_P = +\lambda_\parallel[\sin(k_x a)\sigma_x\tau_x + \sin(k_y a)\sigma_y\tau_x].$$

In the calculation, the parameters are set to be $m_0 = 0.28$ eV; $t_\perp = 0.4$ eV; $t_\parallel = 0.566$ eV; $\lambda_\perp = 0.44$ eV; $\lambda_\parallel = 0.41$ eV. The lattice constants are set to be $a = b = 1.0$ nm and $c = 0.5$ nm. For a film of finite thickness $L_z = N_z c$, $i_z = 1, \ldots, N_z$.

The energy dispersions can be obtained by diagonalizing the Hamiltonian for a finite number of layers $N_z$. A finite gap $\Delta_0$ opens for the gapless Dirac cone and decays exponentially in the thickness of the film. A finite exchange interaction can reduce the gap further. For $L_z = 10$ nm, $\Delta_0 = 2.21 \times 10^{-6}$ eV for $V_z = 0$, and $\Delta_0 = 2.17 \times 10^{-10}$ eV for $V_z = 0.1$ eV. Thus the gap is negligibly tiny.

### 2. Zero modes

To gain an intuitive picture about the surface states of the topological insulator, we put aside the $\lambda_\parallel$ term and reduce the Hamiltonian for a thin film to the $k$-dependent one-dimensional lattice model

$$
\begin{aligned}
H_{\mathrm{1d}}(k) = \sum_{i_z} &\Psi_{i_z,\mathbf{k}}^\dagger M_0(\mathbf{k})\sigma_0\tau_z\Psi_{i_z,\mathbf{k}} \\
&+ \Psi_{i_z,\mathbf{k}}^\dagger\left(t_\perp\sigma_0\tau_z - i\frac{\lambda_\perp}{2}\sigma_z\tau_x\right)\Psi_{i_z+1,\mathbf{k}} + \mathrm{H.c.},
\end{aligned}
$$

where $M_0(\mathbf{k}) = m_0(\mathbf{k}) - 2t_\perp = m_0 - 2t_\perp - 4t_\parallel(\sin^2\frac{k_x a}{2} + \sin^2\frac{k_y a}{2})$. The Hamiltonian has the good quantum number $s = \pm 1$, which is the eigenvalue of $\sigma_z$. In each block of Hamiltonian $H_{\mathrm{1d}}^s$, one can obtain the zero modes of the model in the open boundary condition.

We now solve the zero modes of a semi-infinite chain ($i_z = 1, 2, 3, \ldots,$). With the basis $[\Psi_{1,\mathbf{k}}, \Psi_{2,\mathbf{k}}, \Psi_{3,\mathbf{k}}, \ldots,]^T$, the

Hamiltonian is

$$H_{1d}^s(k) = \begin{bmatrix} M_0(\mathbf{k})\tau_z & t_\perp \tau_z - i\frac{\lambda_\perp}{2}s\tau_x & 0 & 0 & \cdots \\ t_\perp \tau_z + i\frac{\lambda_\perp}{2}s\tau_x & M_0(\mathbf{k})\tau_z & t_\perp \tau_z - i\frac{\lambda_\perp}{2}s\tau_x & 0 & \cdots \\ 0 & t_\perp \tau_z + i\frac{\lambda_\perp}{2}s\tau_x & M_0(\mathbf{k})\tau_z & \ddots & \ddots \\ 0 & 0 & \ddots & \ddots & \ddots \\ \vdots & \vdots & & \ddots & \ddots & \ddots \end{bmatrix}. \tag{A2}$$

The zero modes are the solution of the recurrence equations

$$\left(t_\perp \tau_z + i\frac{\lambda_\perp}{2}s\tau_x\right)\Psi_{i_z-1,\mathbf{k}} + M_0(\mathbf{k})\tau_z\Psi_{i_z,\mathbf{k}} + \left(t_\perp \tau_z - i\frac{\lambda_\perp}{2}s\tau_x\right)\Psi_{i_z+1,\mathbf{k}} = 0. \tag{A3}$$

Set the trial function $\Psi_{i_z,\mathbf{k}} = \beta\Psi_{i_z-1,\mathbf{k}} = \beta^{i_z}\Psi_{\mathbf{k}}$. The equation is reduced to

$$\left[\left(t_\perp \tau_z + i\frac{\lambda_\perp}{2}s\tau_x\right) + M_0(\mathbf{k})\tau_z\beta + \left(t_\perp \tau_z - i\frac{\lambda_\perp}{2}s\tau_x\right)\beta^2\right]\Psi_{\mathbf{k}}$$
$$= 0. \tag{A4}$$

Multiplied by $\tau_z$, it follows that $\Psi_{\mathbf{k}}$ should be the eigenstate of $\tau_y$, $\Psi_{\mathbf{k}} = \chi_t \Phi_{\mathbf{k}}$, where $\chi_t$ is the eigenvector of $\tau_y$ with the eigenvalue $t = \pm 1$. Thus

$$\left(t_\perp - \frac{\lambda_\perp}{2}st\right) + M_0(\mathbf{k})\beta + \left(t_\perp + \frac{\lambda_\perp}{2}st\right)\beta^2 = 0. \tag{A5}$$

Two roots of $\beta$ are

$$\beta_\pm = \frac{-M_0(\mathbf{k}) \pm \sqrt{M_0^2(\mathbf{k}) - 4\left(t_\perp^2 - \frac{\lambda_\perp^2}{4}\right)}}{2\left(t_\perp + \frac{\lambda_\perp}{2}st\right)}. \tag{A6}$$

The boundary conditions $\Psi_{i_z=0,\mathbf{k}} = 0$ and $\Psi_{i_z\to\infty,\mathbf{k}} \to 0$ require $|\beta_\pm| < 1$. Thus

$$|\beta_+\beta_-| = \left|\frac{t_\perp - \frac{\lambda_\perp}{2}st}{t_\perp + \frac{\lambda_\perp}{2}st}\right| < 1, \tag{A7}$$

which leads to $st = \mathrm{sgn}[t_\perp\lambda_\perp]$. Hence, the zero modes are the eigenvectors of $\sigma_z\tau_y$ with eigenvalues $st = 1$ ($s = t = 1$ and $s = t = -1$).
$|\beta_\pm| < 1$ further requires

$$\left|-M_0(\mathbf{k}) \pm \sqrt{M_0^2(\mathbf{k}) - 4\left(t_\perp^2 - \frac{\lambda_\perp^2}{4}\right)}\right| < 2\left(t_\perp + \frac{\lambda_\perp}{2}\right), \tag{A8}$$

which leads to $-2t_\perp < M_0(\mathbf{k}) < 2t_\perp$. Hence, the zero modes exist for $k$ satisfying

$$0 < m_0 - 4t_\parallel\left(\sin^2\frac{k_x a}{2} + \sin^2\frac{k_y a}{2}\right) < 4t_\perp. \tag{A9}$$

Thus, the wave function of the zero modes are

$$\Psi_{i_z,\mathbf{k}} = (\beta_+^{i_z} - \beta_-^{i_z})\Phi_{\mathbf{k}}\xi_s \otimes \chi_t, \tag{A10}$$

with $st = 1$, and $(k_x^2 + k_y^2)a^2 < k_c^2 a^2 \simeq m_0/t_\parallel$.

By the same token, the condition of $st = -1$ gives two zero modes in the opposite end. One can notice that $\beta_\pm$ have an interesting property, i.e., when $M_0^2(\mathbf{k}) - 4(t_\perp^2 - \frac{\lambda_\perp^2}{4}) < 0$, $\beta_\pm$ are complex. In this regime, as shown in Fig. 6, their modulus is a constant

$$|\beta_\pm|^2 = \frac{\left(t_\perp^2 - \frac{\lambda_\perp^2}{4}\right)}{\left(t_\perp + \frac{\lambda_\perp}{2}\right)^2}. \tag{A11}$$

In this regime, the zero modes in every $k$ point are as localized as the zero modes at the $\Gamma$ point. Hence, the exchange field on one surface will not affect the other surface. We called this regime the "parity-invariant regime." The property of $\beta_\pm$ in this regime explains why the Hall conductance is quantized as a plateau.

### 3. Effective model

The lowest four bands of the semi-magnetic topological insulator thin film can be effectively described by a $4 \times 4$
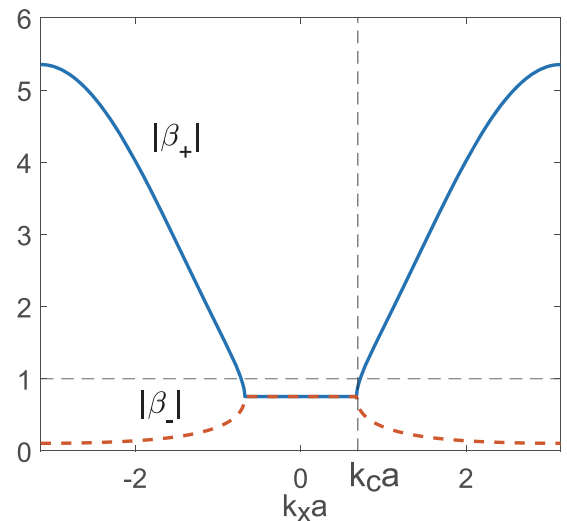


FIG. 6. The modulus of $\beta_\pm$ depending on $k_x$ with $k_y = 0$. The plateau of the modulus equals to $\sqrt{t_\perp^2 - \frac{\lambda_\perp^2}{4}}/(t_\perp + \frac{\lambda_\perp}{2})$.

Hamiltonian in a two-dimensional Brillouin zone

$$H_F = \begin{pmatrix} \lambda_{\parallel}(\sin k_x a \sigma_y - \sin k_y a \sigma_x) + V(\mathbf{k})\sigma_z & f[m_0(\mathbf{k})/T^*]m_0(\mathbf{k}) \\ f[m_0(\mathbf{k})/T^*]m_0(\mathbf{k}) & -\lambda_{\parallel}(\sin k_x a \sigma_y - \sin k_y a \sigma_x) \end{pmatrix}, \quad (A12)$$

where $V(\mathbf{k}) = V_0 f[-m_0(\mathbf{k})/T^*] + V_1 f[m_0(\mathbf{k})/T^*]$ and $m_0(\mathbf{k}) = m_0 - 4t_{\parallel}(\sin^2 \frac{k_x a}{2} + \sin^2 \frac{k_y a}{2})$. The Fermi-Dirac-distribution-like factor $f(x) = [\exp(x) + 1]^{-1}$ describes the process that the surface states merge into the bulk states. The coefficient $T^*$ is a model-specific parameter. The Brillouin zone is divided into two regimes by the sign of $m_0(\mathbf{k})$. Here $k_c a \simeq 0.69$, which is given by $m_0(\mathbf{k}_c) = 0$. $f(k) = 0$ in a wide range area of momentum space $k_{\parallel}^2 < k_c^2$, which is the parity-invariant regime as we mentioned above. $f(k) = 1$ in the outside $k_{\parallel}^2 > k_c^2$, where the top and bottom surface states are coupled via the term $m_0(\mathbf{k})$.

The top surface states experience the exchange field $V_0$ and the field decays to a constant $V_1$ when momentum exceeds $k_c$. The parameters are $V_0 = V_z = 0.1$eV, and $V_1/V_0 \simeq L_z^{\mathrm{Mag}}/L_z \ll 1$ where $L_z^{\mathrm{Mag}}$ is the thickness of the magnetically doped film. Figure 7 compares the results of the effective model to the numerical results of the thin film by setting $T^* = 0.05t_{\parallel}$ here. The energy separation between the gapped and gapless bands shows the same dip at $k_c$. The Hall conductance of the gapless band exhibits the half-quantized Hall conductance in a wider range as a function of the Fermi energy level, and the gapped band shows the zero Hall conductance when the valence bands are fully filled. The total Hall conductance is half quantized near the energy crossing point as expected.

The eigenstates for Hamiltonian (A12) are

$$|\Psi_{S=+,s}\rangle = \begin{pmatrix} \cos\frac{\varphi_{\mathbf{k}}}{2}|\psi_{S=+,s}\rangle \\ -\sin\frac{\varphi_{\mathbf{k}}}{2}\sigma_z|\psi_{S=+,s}\rangle \end{pmatrix},$$

$$|\Psi_{S=-,s}\rangle = \begin{pmatrix} \sin\frac{\varphi_{\mathbf{k}}}{2}\sigma_z|\psi_{S=-,s}\rangle \\ \cos\frac{\varphi_{\mathbf{k}}}{2}|\psi_{S=-,s}\rangle \end{pmatrix},$$
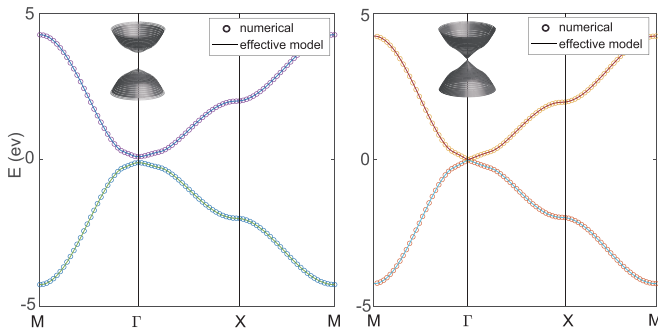


FIG. 7. Comparison between numerical calculated spectra and the spectra of the effective model. The circles are the numerical results, the solid line are the results of effective model. Left: The gapped bands. Right: The gapless bands. The numerical calculation is on the 10-nm film where the top 2-nm layers are Cr doped with $V_z = 0.1$eV. The parameters are $m_0 = 0.28$ eV; $t_\perp = 0.4$ eV; $t_{\parallel} = 0.566$ eV; $\lambda_\perp = 0.44$ eV; $\lambda_{\parallel} = 0.41$ eV [35]. The thickness $L_z = 10$ nm. The lattice constants are $a = b = 1.0$ nm and $c = 0.5$ nm. The parameter for the effective model is $T^* = 0.05t_{\parallel}$.

with the two-component spinors

$$|\psi_{S,-}\rangle = \begin{pmatrix} iS\sin\frac{\phi_S}{2} \\ \cos\frac{\phi_S}{2}e^{i\theta_{\mathbf{k}}} \end{pmatrix}, \quad |\psi_{S,+}\rangle = \begin{pmatrix} -iS\cos\frac{\phi_S}{2} \\ \sin\frac{\phi_S}{2}e^{i\theta_{\mathbf{k}}} \end{pmatrix},$$

and the corresponding eigenvalues are $s\varepsilon_S$ with $\varepsilon_S = \sqrt{\lambda_{\parallel}^2[\sin^2(k_x a) + \sin^2(k_y a)] + M_S^2(k)}$ where $s = \pm$ denote the conduction and valence bands, respectively, and $S = \pm$ denote the two states in the conduction and valence band. Here $M_S = \frac{1}{2}V(\mathbf{k}) + S\sqrt{\{f[\frac{m_0(\mathbf{k})}{T^*}]m_0(\mathbf{k})\}^2 + \frac{1}{4}V^2(\mathbf{k})}$, $\varphi_{\mathbf{k}} = \arctan\frac{f[\frac{m_0(\mathbf{k})}{T^*}]m_0(\mathbf{k})}{\frac{1}{2}V(\mathbf{k})}$ and $\cos\phi_S = \frac{M_S}{\varepsilon_S}$.

We then evaluate the Berry connection and the Berry curvature in the continuum limit, which allows us to perform the calculations in polar coordinates. Since the radial component of the Berry connection is only a function of radial coordinate $k$ and thus does not contribute to the Berry curvature along the $z$ direction. We only need to evaluate the angular part of the Berry connection

$$A_\theta^{S,s;S,s} = -i\frac{1}{k}\langle\Psi_{S,s}|\partial_\theta|\Psi_{S,s}\rangle = \frac{1}{k}\frac{1 - s\cos\phi_S}{2}.$$

Then the Berry curvature along the $z$ direction is given by

$$\Omega_z^{S,s;S,s} = \frac{1}{k}\left(\frac{\partial(kA_\theta^{S,s;S,s})}{\partial k} - \frac{\partial A_k^{S,s;S,s}}{\partial\theta}\right) = -\frac{s}{2k}\partial_k\cos\phi_S. \quad (A13)$$

The total Hall conductance is $\sigma_H = \sum_{S,s}\sigma_H^{S,s}$ with the Hall conductance for each band as

$$\sigma_H^{S,s} = \frac{e^2}{h}\int\frac{d^2\mathbf{k}}{2\pi}\Omega_z^{S,s;S,s}\theta[\mu_F - s\varepsilon_S(k)].$$

From Eq. (A13), for the valence bands $s = -$, we have

$$\sigma_H^{S,-} = \frac{e^2}{2h}[S - \cos\phi_S(k_F^{S,-})],$$

where $k_F^{S,s}$ is the Fermi wave vector for each band and $k_F^{S,s} = 0$ for a fully filled band.

### 4. Comparison between numerical results and the effective model

In this section, we present the spectra and the Berry curvature of the numerical results for the model in Eq. (1) and the effective model in Eq. (3). The numerical results are obtained by solving the quasi-two-dimensional tight-binding model numerically. We focus on the four bands which are associated with the surface states of the thin film. The energy spectra of the effective Hamiltonian (A12) are

$$\varepsilon_S^2 = \lambda_{\parallel}^2(\sin^2 k_x a + \sin^2 k_y a) + \left(V(k)/2 + S\sqrt{V^2/4 + [f(m_0(\mathbf{k})/T^*)m_0(\mathbf{k})]^2}\right)^2,$$

with $S = \pm$. There are two gapped and two gapless bands. The analytical and numerical results are in excellent agreement as shown in Fig. 7.
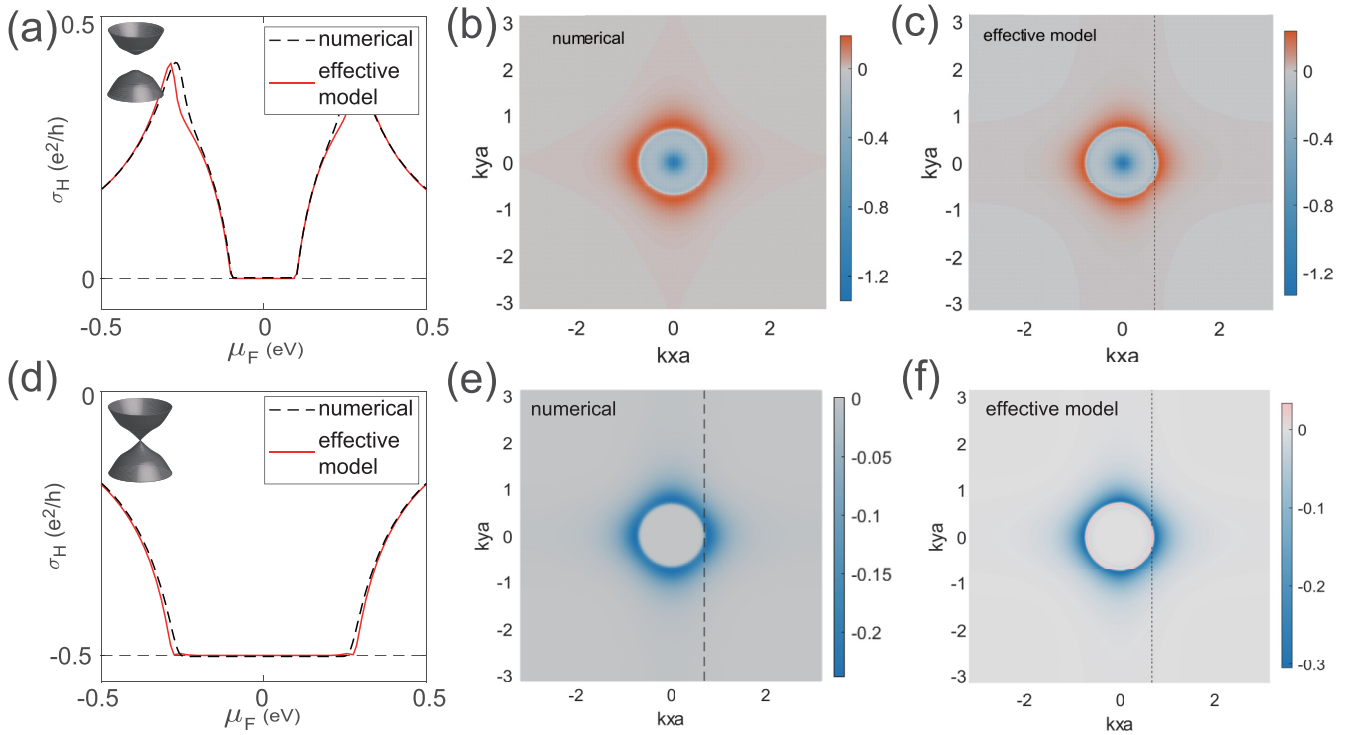
FIG. 8. Comparison of the Berry curvatures of the gapless and gapped bands. (a) The Hall conductance of the gapped band depending on Fermi level. (b) The Berry curvature distribution of the gapped valence band by numerical calculation. (c) The Berry curvature distribution of the gapped valence band using the effective model. (d) The Hall conductance of the gapless band depending on Fermi level. (e) The Berry curvature distribution of the gapless valence band by numerical calculation. (f) The Berry curvature distribution of the gapless valence band using the effective model.

We further present the Hall conductance and the Berry curvature for the gapped and gapless bands in Fig. 8. The Hall conductance is zero for the gapped bands when the Fermi level lies between the band gap caused by the exchange interaction while the Hall conductance is $-1/2$ for the gapless bands when the Fermi level lies between the bulk band gap. The later is much larger. The Berry curvatures for the two bands are also presented for comparison.

### 5. Laughlin-like argument for the half-quantized Hall conductance in semi-magnetic topological insulator

In this section, we discuss how to understand the half-quantized Hall conductance in a semi-magnetic topological insulator following Laughlin's argument. Here we consider the periodic direction $x$ is bent into a Corbino disk and pierced by a magnetic flux $\Phi$ for three different cases as shown in the upper panel of Fig. 9: (a) the quantum anomalous Hall state that the topological insulator thin-film is coated by magnetic layers on both its top and bottom surfaces with parallel magnetization; (b) the semimetal state that only top surface is coated with magnetic layers; and (c) the axion insulating state that the magnetizations of the coated two magnetic layers are antiparallel. Then we discuss the charge transfer between inner and outer perimeters (green surfaces in in the upper panel of Fig. 9) if the flux changes by a quantum flux $\Delta\Phi = \Phi_0 = h/e$ over time $\Delta t$.

For a changing flux, an electric field along the circumferential direction is induced according to Faraday's law, $E(t) = \frac{1}{2\pi R}\partial_t \Phi$ with $R$ as the radial distance from the center of the Corbino disk. Due to the boundary confinement effect along the $y$ directions, the energy spectra of the surface states for such a geometry become a series of discrete one-dimensional subbands. As shown in the lower panel of Fig. 9(a), in the quantum anomalous Hall state there exist counterpropagating chiral edge modes localized at the inner and outer surfaces within the magnetic gap (denoted by the green shadow region). The wave-function distribution in the $y$ direction for each state $\langle y/L_y \rangle$ is indicated by the blue to red color gradient. If we now change the threading flux, this corresponds to a change in the vector potential in the circumferential direction $x$. This gauge change shifts the center of the wave function by an amount $e\Delta A$ with $\Delta A$ being the gauge change. In particular, the Hamiltonian and the spectra remain the same after changing the flux of $\Phi_0$. The shift moves each state precisely to an adjacent center. The only change induced by the adiabatic insertion of a quantized flux is to carry the system from one eigenstate to another, denoted by the dashed blue and red arrows. In this situation, the net effect is to move one electron from one edge to the other. The entire charge transfer of one electron is $\Delta Q = e$ between the edges as the flux changes by $\Delta\Phi = \Phi_0$ which corresponds a quantized Hall conductance from $\Delta Q = \sigma_H \Delta\Phi$ [26,50]. However, in the semi-metal case, as shown in the lower panel of Fig. 9(b), the Fermi level $\mu_F$ (denoted by the blue dashed line) crosses a series of subbands
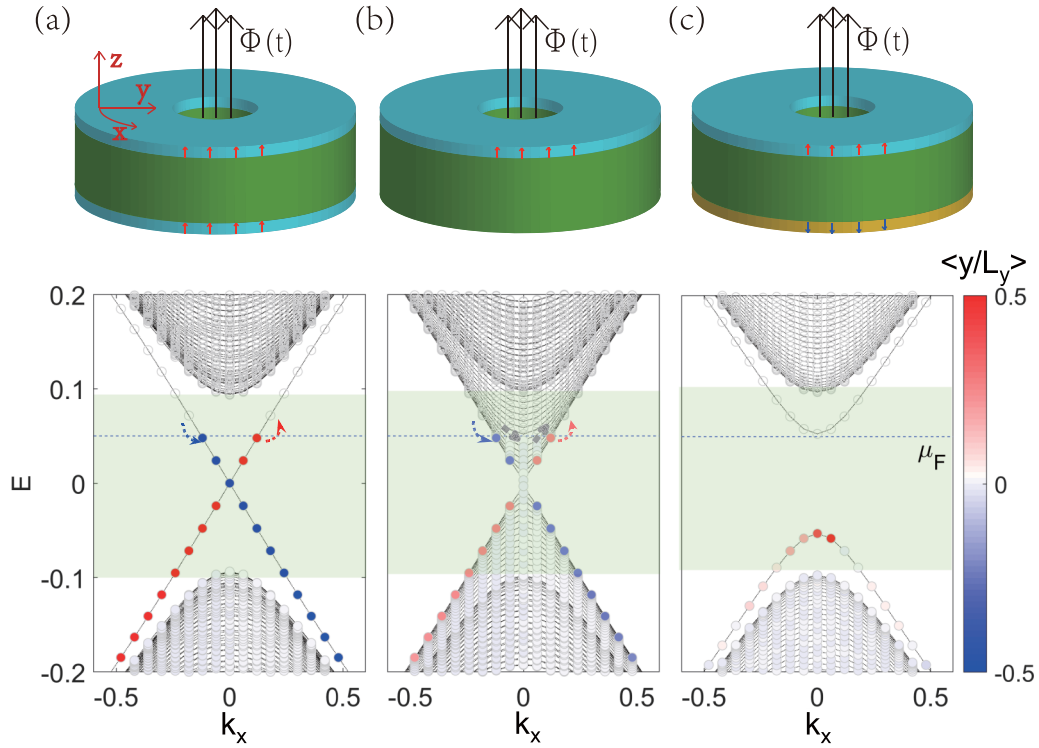
FIG. 9. The upper panel shows the setups for Laughlin's argument for (a) the quantum anomalous Hall state, (b) the semi-magnetic topological insulator, and (c) the axion insulator state. A time-dependent flux $\Phi(t)$ threads in the ring's hole. The lower panel shows the energy spectrum for the corresponding cases. The blue-to-red color gradient represents the wave-function distribution $\langle y/L_y \rangle$ in the $y$ direction for each state. The dashed arrows indicate the movement of the relevant states as the adiabatic change of a quantum flux. The blue dashed lines indicate the Fermi level $\mu_F$. The exchange-field-induced magnetic gap for the surface states are indicated by the green shadow region.

from the gapless bottom surface states instead of only two edge states in the quantum anomalous Hall state. These states are distributed extensively over the bottom surface. By examining the position expectation of each state $\langle y/L_y \rangle$, one finds that the clockwise-propagating states are located close to the inner perimeter and the anticlockwise-propagating states are located close to the outer perimeter. The adiabatic change of quantum flux moves the states for all the subbands crossed by the chemical potential (denoted by the arrows) and the charge transfer from outer side to the inner side can be evaluated from the spatial imbalance difference between all the states with opposite velocity at the Fermi level [34] $\Delta Q = -\frac{e}{2}$. Thus, the change of a quantum flux moves a half charge from one edge to the other. This one-half charge transfer is a collective result from all the bands intersecting the Fermi level. It is in sharp contrast to the quantum anomalous insulator where the contribution comes only from the two chiral edge states and there are no net particle creations or annihilations in the other modes. For the axion-insulating state shown as the lower panel of Fig. 9(c), the Fermi level crosses no bands, there is no charge transfer as the change of the flux, and the Hall conductance is zero.

### 6. Robustness of the Hall conductance in the presence of disorder

We study the robustness of the half-quantized Hall conductance in the presence of disorder by means of the effective

model and the self-consistent Born approximation. Here we consider the randomly distributed, spin- and orbital-independent scalar-type disorder potential: $H_{\mathrm{dis}} = V(\mathbf{r}) 1_4$ with $V(\mathbf{r}) = \sum_{i=1}^{N_i} u_0 \delta_{\mathbf{r},\mathbf{r}_i}^2 \delta_{z,z_i}$, the scatterers of $\pm u_0$ are randomly distributed with equal probability, and $N_i$ impurities are randomly located among $N = N_x N_y N_z$ lattices with the impurity density as $n_i = N_i/N$. To facilitate the calculation, we first perform a unitary transformation $U(\mathbf{k}) = e^{-i\tau_y \sigma_z \varphi_{\mathbf{k}}/2}$ with $\varphi_{\mathbf{k}} = \arctan \frac{f[\frac{m_0(\mathbf{k})}{T^*}]m_0(\mathbf{k})}{\frac{1}{2}V(\mathbf{k})}$ such that the Hamiltonian can be brought into a block-diagonalized form

$$H_F' = U H_F U^{-1} = \begin{pmatrix} H_+ & 0 \\ 0 & H_- \end{pmatrix}, \qquad \text{(A14)}$$

where

$$H_{S'} = S' \lambda_{||} (\sin k_x a \sigma_y - \sin k_y a \sigma_x) + M_{S'}(\mathbf{k}) \sigma_z.$$

Here $M_{S'}(\mathbf{k}) = g(\mathbf{k})(S' + \cos \varphi_{\mathbf{k}})$ and $g(\mathbf{k}) = \sqrt{[f[\frac{m_0(\mathbf{k})}{T^*}]m_0(\mathbf{k})]^2 + \frac{1}{4}V(\mathbf{k})^2}$. The basis is transformed as $|\Psi_{S',s'}'(\mathbf{k})\rangle = \sum_{S,s} U_{S',s';S,s}(\mathbf{k})|\Psi_{S,s}\rangle$ where the symbols with a prime denote the new basis for $H_F'$ after the transformation. In the original basis, the capital letters $S = \pm$ denotes the top and bottom surfaces, respectively, and the lowercase letters $s = \pm$ denote the two bases for each surface. The scattering

matrix in the transformed basis is

$$V_{\mathbf{k},\mathbf{k}'}^{R',r';S',s'} = \langle \Psi'_{R',r'}(\mathbf{k})|V(\mathbf{r})|\Psi'_{S',s'}(\mathbf{k}')\rangle$$

$$= \sum_{i=1}^{N_i} u_0 \frac{e^{-i(\mathbf{k}-\mathbf{k}')\cdot\mathbf{r}_i}}{N_x N_y} \sum_{S,s} U^*_{R',r';S,s}(\mathbf{k}) U_{S',s';S,s}(\mathbf{k}')\phi^*_S(z_i)\phi_S(z_i),$$

where we use $\langle \xi_r|\xi_s\rangle\langle \chi_{Rr}|\chi_{Ss}\rangle = \delta_{RS}\delta_{rs}$ for the scalar potentials and $\phi_S(z)$ is the wave function in the $z$ direction with $\sum_z \phi^*_R(z)\phi_S(z) = \delta_{RS}$, which is orthonormal in surface subspace. The disorder averaging of two scattering matrix elements can be evaluated as [46]

$$\langle V_{\mathbf{k},\mathbf{k}'}^{R',r';S',s'} V_{\mathbf{k}',\mathbf{k}}^{S',s';R',r'}\rangle_{\mathrm{dis}} = \frac{n_i u_0^2}{N} \left( \sum_{S,s} U^*_{R',r';S,s}(\mathbf{k}) U_{S',s';S,s}(\mathbf{k}') \right) \left( \sum_{Q,q} U_{R',r'';Q,q}(\mathbf{k}) U^*_{S',s'';Q,q}(\mathbf{k}') \right).$$

From $U(\mathbf{k})U^{-1}(\mathbf{k}') = e^{-i\tau_y\sigma_z(\varphi_{\mathbf{k}}-\varphi_{\mathbf{k}'})/2}$, the intra and intersubblock disorder-averaged scattering amplitude can be obtained as

$$\langle V_{\mathbf{k}\mathbf{k}'}^{R',R'} \otimes V_{\mathbf{k}'\mathbf{k}}^{R',R'}\rangle_{\mathrm{dis}} = \frac{1 + \cos(\varphi_{\mathbf{k}} - \varphi_{\mathbf{k}'})}{2}\sigma_0 \otimes \sigma_0,$$

$$\langle V_{\mathbf{k}\mathbf{k}'}^{R',-R'} \otimes V_{\mathbf{k}'\mathbf{k}}^{-R',R'}\rangle_{\mathrm{dis}} = \frac{1 - \cos(\varphi_{\mathbf{k}} - \varphi_{\mathbf{k}'})}{2}\sigma_z \otimes \sigma_z.$$

In the self-consistent Born approximation (SCBA), the self-energy $\Sigma_{R'R'}(E, \mathbf{k})$ for each subblock is given by [51]

$$\Sigma_{R'R'}(E, \mathbf{k}) = \sum_{S'} \sum_{\mathbf{k}'} \left\langle V_{\mathbf{k},\mathbf{k}'}^{R'S'} \frac{1}{E - \Sigma_{S'}(E, \mathbf{k}') - H_{S'}(\mathbf{k}')} V_{\mathbf{k}',\mathbf{k}}^{S'R'}\right\rangle_{\mathrm{dis}}.$$

The subblock self-energy $\Sigma_{R'R'}$ can be decomposed into Pauli matrices $\Sigma_{R'R'} = \sum_{i=0,x,y,z} \Sigma^i_{R'R'}\sigma_i$. The renormalized Dirac mass for subblock $S'$ is given by

$$\bar{M}_{S'}(\mathbf{k}) = M_{S'}(\mathbf{k}) + \Sigma^z_{S'S'}(0, \mathbf{0}) = g(\mathbf{k})\big(S' + \cos\varphi_{\mathbf{k}}\big) + \Sigma^z_{S'S'}(0, \mathbf{0}).$$

Here we only are interested in mass renormalization for the gapless subblock which restricts us to only consider the self-energy $\Sigma_{--}$ for the lower subblock in Eq. (A14),

$$\Sigma^z_{--}(0, \mathbf{0}) = \frac{1}{2}\sum_{S'=\pm}\sum_{\mathbf{k}'} \frac{\mathrm{Tr}\big[\sigma_z\langle V_{\mathbf{0},\mathbf{k}'}^{-,S'}\bar{H}_{S'}(\mathbf{k}')V_{\mathbf{k}',\mathbf{0}}^{S',-}\rangle_{\mathrm{dis}}\big]}{-\bar{\varepsilon}^2_{S'}(\mathbf{k}')}$$

$$= \frac{1}{2}\frac{n_i u_0^2 \mathrm{v}_0}{L_z}\int \frac{d^2\mathbf{k}'}{(2\pi)^2}\left(\frac{1 - \cos\varphi_{\mathbf{k}'}}{2}\frac{\bar{M}_+(\mathbf{k}')}{-\bar{\varepsilon}^2_+(\mathbf{k}')} + \frac{1 + \cos\varphi_{\mathbf{k}'}}{2}\frac{\bar{M}_-(\mathbf{k}')}{-\bar{\varepsilon}^2_-(\mathbf{k}')}\right),$$

where $L_z$ is the thickness of the sample, $\mathrm{v}_0 = a^3$ is the volume of the unit cell, and $\bar{\varepsilon}_{S'} = \sqrt{\lambda_\parallel^2 \sum_{i=x,y}\sin k_i a + \bar{M}^2_{S'}(\mathbf{k})}$ is the renormalized dispersion. For weak disorder strength, the renormalized functions in the integral can be approximated by the unrenormalized ones

$$\Sigma^z_{--}(0, \mathbf{0}) = \frac{1}{2}\frac{n_i u_0^2 \mathrm{v}_0}{L_z}\int \frac{d^2\mathbf{k}'}{(2\pi)^2}g(\mathbf{k}')(1 - \cos^2\varphi_{\mathbf{k}'})\frac{1}{2}\left(\frac{1}{\varepsilon^2_-(\mathbf{k}')} - \frac{1}{\varepsilon^2_+(\mathbf{k}')}\right)$$

$$= \frac{n_i u_0^2 \mathrm{v}_0}{L_z}\int \frac{d^2\mathbf{k}'}{(2\pi)^2}\sin^2\varphi_{\mathbf{k}'}\cos\varphi_{\mathbf{k}'}\frac{g^3(\mathbf{k}')}{\varepsilon^2_-(\mathbf{k}')\varepsilon^2_+(\mathbf{k}')}. \tag{A15}$$

For $|\mathbf{k}| < k_c$, we have $\sin\varphi_{\mathbf{k}} \sim 0$. In this parity-invariant regime $|\mathbf{k}| < k_c$, the Dirac mass renormalization is attributed to the impurity scatterings from the undoped bottom surface states. Since we have $\sin\varphi_{\mathbf{k}} \sim 0$ for $|\mathbf{k}| < k_c$, this part of the contribution in Eq. (A15) vanishes as a direct consequence of the local time-reversal symmetry. In the parity-breaking regime $|\mathbf{k}| > k_c$, the contribution of the integration comes from the surface-to-bulk scattering. In this regime, there is no symmetry to guarantee the vanishing of the integral. However, as the magnetic element is doped on the top few layers this only causes a Zeeman energy splitting in the order of $V_0 L_z^{\mathrm{Mag}}/L_z$ for the bulk states. In this regime, the gapped and gapless bands are nearly degenerate and give the contributions to the integral which alternate in sign. The total contributions from these two bands yield a prefactor $\cos\varphi_{\mathbf{k}'}$. For $|\mathbf{k}| > k_c$,

we have $\varphi_{\mathbf{k}} = \arctan\frac{2m_0(\mathbf{k})}{V_1} \sim \arctan(\frac{2m_0(\mathbf{k})}{V_0}\frac{L_z}{L_z^{\mathrm{Mag}}})$. The presence of the factor $\frac{L_z}{L_z^{\mathrm{Mag}}} \gg 1$ yields the results $\varphi_{\mathbf{k}} \sim \pi/2$ and $\cos\varphi_{\mathbf{k}} \sim 0$. The integral Eq. (A15) is strongly suppressed due to the factor $\sin^2\varphi_{\mathbf{k}'}\cos\varphi_{\mathbf{k}'}$. As a consequence, the integral in Eq. (A15) nearly vanishes for large $L_z$, which explains the robustness of the half-quantized Hall conductance in the presence of weak disorder. The underlying physics can be understood in a more intuitive way. The presence of impurities causes the scattering between the electron wave functions which lead to a level-repulsion effect [48]. The stability of the Dirac point is thus equivalent to examining the relative level repulsion between the two states at the Dirac point from all other surface and bulk states. The scattering between two bottom surface states will not renormalize the Dirac mass

due to the presence of the local time-reversal symmetry. The scattering from the top surface states can also be neglected due to the fact that the two opposite surface states have an exponentially small overlap. The magnetic doping on the top surface will cause an energy splitting $\sim V_z L_z^{\mathrm{mag}}/L_z$ for the two degenerate bulk states with the thickness of the magnetic layer $L_z^{\mathrm{mag}}$. For a sufficiently small ratio of $L_z^{\mathrm{mag}}/L_z$, the level repulsion effect from two nearly degenerate bulk states will be canceled out.

To demonstrate how the gapless Dirac cone can be stabilized due to the existence of the massive Dirac cone in the presence of disorder, we also calculate the disorder-induced self-energy correction for two-dimensional gapless Wilson Fermion as a comparison. In momentum representation, the tight-binding Hamiltonian for a two-dimensional gapless Wilson fermion can be expressed as [11]

$$H_{\mathrm{WF}} = \mathbf{d}(\mathbf{k}) \cdot \boldsymbol{\sigma},$$

with

$$\mathbf{d} = \left( \frac{\hbar v}{a} \sin(k_x a), \frac{\hbar v}{a} \sin(k_y a), \frac{4b\hbar^2}{a^2} \sum_{i=x,y} \sin^2 \left( \frac{k_i a}{2} \right) \right).$$

In the self-consistent Born approximation, the self-energy $\Sigma_{\mathrm{WF}} = \sum_{i=0,x,y,z} \Sigma_{\mathrm{WF}}^i \sigma^i$ is a $2 \times 2$ matrix which is given by the integral [49]

$$\Sigma_{\mathrm{WF}} = n_i u_0^2 a^2 \int \frac{d^2 \mathbf{k}}{(2\pi)^2} \frac{1}{E - H_{\mathrm{WF}}(\mathbf{k}) - \Sigma_{\mathrm{WF}}}. \quad (A16)$$

Here we only consider the mass renormalization $\mathrm{Re}\Sigma_{\mathrm{WF}}^z(E = 0)$, then Eq. (A16) becomes

$$\Sigma_{\mathrm{WF}}^z = -n_i u_0^2 a^2 \int \frac{d^2 \mathbf{k}}{(2\pi)^2} \frac{b\hbar^2 \mathbf{k}^2 + \Sigma_{\mathrm{WF}}^z}{\hbar^2 v^2 \mathbf{k}^2 + \left( b\hbar^2 \mathbf{k}^2 + \Sigma_{\mathrm{WF}}^z \right)^2},$$

where we use the continuum limit $\mathbf{d} = (\hbar v k_x, \hbar v k_y, b\hbar^2 \mathbf{k}^2)$. Without introducing the high-energy cutoff, this integral dis-

plays a logarithmic ultraviolet divergence which indicates that the states with higher energy give larger contributions to the integral. This behavior is distinctly different from Eq. (A15) for the four-band model where the higher-energy contributions are canceled due to the existence of an additional massive Dirac band. By introducing the high momentum cutoff $\Lambda \sim \hbar \pi / a$, the integral can be evaluated as

$$\Sigma_{\mathrm{WF}}^z \approx -\mathrm{sgn}(b) \frac{\pi}{4} \frac{n_i u_0^2}{E_c} \ln \left( \frac{E_c}{|\Sigma_{\mathrm{WF}}^z|} \right),$$

where $E_c = |b|\hbar^2 \Lambda^2 \gg \hbar v \Lambda$, $\Sigma_{wf}^z$ is the largest energy scale in the problem. This transcendental equation can be solved as

$$\Sigma_{\mathrm{WF}}^z = -\mathrm{sgn}(b) E_c \exp \left[ -W \left( \frac{4}{\pi} \frac{E_c^2}{n_i u_0^2} \right) \right],$$

where $W$ is the product logarithm function. For the value of argument, $W(x)$ is asymptotic as $W(x) \sim \ln x - \ln \ln(x)$. By introducing the dimensionless disorder strength $\kappa = \frac{\pi}{4} \frac{n_i u_0^2}{E_c^2}$, we have

$$\Sigma_{\mathrm{WF}}^z \sim -\mathrm{sgn}(b) E_c \kappa \ln \left( \frac{1}{\kappa} \right),$$

that a sufficiently weak disorder will drive the gapless Wilson fermion into a topological insulator phase with a Dirac mass $\Sigma_{\mathrm{WF}}^z$.

In comparison with the two-band model [49], the contributions to the Dirac mass renormalization from the gapped and gapless bands in the four-band model in Eq. (A14) alternate in sign and cancel each other out at high energy. As a consequence, the Dirac point is still stable against disorder due to the local time-reversal symmetry and the accompanying gapped bands.

[1] S. Murakami, Phase transition between the quantum spin Hall and insulator phases in 3D: Emergence of a topological gapless phase, New J. Phys. **9**, 356 (2007).

[2] B. J. Yang and N. Nagaosa, Classification of stable three-dimensional Dirac semimetals with nontrivial topology, Nat. Commun. **5**, 4898 (2014).

[3] N. P. Armitage, E. J. Mele, and A. Vishwanath, Weyl and Dirac semimetals in three-dimensional solids, Rev. Mod. Phys. **90**, 015001 (2018).

[4] A. J. Niemi and G. W. Semenoff, Axial-Anomaly-Induced Fermion Fractionization and Effective Gauge-Theory Actions in Odd-Dimensional Space-Times, Phys. Rev. Lett. **51**, 2077 (1983).

[5] R. Jackiw, Fractional charge and zero modes for planar systems in a magnetic field, Phys. Rev. D **29**, 2375 (1984).

[6] A. N. Redlich, Gauge Noninvariance and Parity Nonconservation of Three-Dimensional Fermions, Phys. Rev. Lett. **52**, 18 (1984).

[7] D. Boyanovsky, R. Blankenbecler, and R. Yahalom, Physical origin of topological mass in 2 + 1 dimensions, Nucl. Phys. B **270**, 483 (1986).

[8] A. M. J. Schakel, Relativistic quantum Hall effect, Phys. Rev. D **43**, 1428 (1991).

[9] H. B. Nielsen and M. Ninomiya, A no-go theorem for regulatizing chiral fermions, Phys. Lett. B **105**, 219 (1981).

[10] K. G. Wilson, *New Phenomena in Subnuclear Physics*, edited by A. Zichichi (Plenum, New York, 1975).

[11] H. J. Rothe, *Lattice Gauge Theories: An Introduction*, 3rd ed. (World Scientific, Singapore, 2005).

[12] G. W. Semenoff, Condensed-Matter Simulation of a Three-Dimensional Anomaly, Phys. Rev. Lett. **53**, 2449 (1984).

[13] E. Fradkin, E. Dagotto, and D. Boyanovsky, Physical Realization of the Parity Anomaly in Condensed Matter Physics, Phys. Rev. Lett. **57**, 2967 (1986).

[14] F. D. M. Haldane, Model for a Quantum Hall Effect without Landau Levels: Condensed-Matter Realization of the "Parity Anomaly," Phys. Rev. Lett. **61**, 2015 (1988).

[15] A. H. Castro Neto, F. Guinea, N. M. R. Peres, K. S. Novoselov, and A. K. Geim, The electronic properties of graphene, Rev. Mod. Phys. **81**, 109 (2009).

[16] K. S. Novoselov, A. K. Geim, S. V. Morozov, D. Jiang, M. I. Katsnelson, I. V. Grigorieva, S. V. Dubonos, and A. A. Firsov,

Two-dimensional gas of massless Dirac fermions in graphene, Nature (London) **438**, 197 (2005).

[17] Y. B. Zhang, Y. W. Tan, H. L. Stormer, and P. Kim, Experimental observation of the quantum Hall effect and Berry's phase in graphene, Nature (London) **438**, 201 (2005).

[18] L. Fu, C. L. Kane, and E. J. Mele, Topological Insulators in Three Dimensions, Phys. Rev. Lett. **98**, 106803 (2007).

[19] M. Z. Hasan, and C. L. Kane, Colloquium: Topological insulators, Rev. Mod. Phys. **82**, 3045 (2010).

[20] X. L. Qi, and S. C. Zhang, Topological insulators and superconductors, Rev. Mod. Phys. **83**, 1057 (2011).

[21] S. Q. Shen, *Topological Insulators*, Springer Series of Solid State Science, Vol. 174 (Springer, Heidelberg, 2012).

[22] L. Fu and C. L. Kane, Topological insulators with inversion symmetry, Phys. Rev. B **76**, 045302 (2007).

[23] X. L. Qi, T. L. Hughes, and S. C. Zhang, Topological field theory of time-reversal invariant insulators, Phys. Rev. B **78**, 195424 (2008).

[24] A. M. Essin, J. E. Moore, and D. Vanderbilt, Magnetoelectric Polarizability and Axion Electrodynamics in Crystalline Insulators, Phys. Rev. Lett. **102**, 146805 (2009).

[25] R. L. Chu, J. R. Shi, and S. Q. Shen, Surface edge state and half-quantized Hall conductance in topological insulators, Phys. Rev. B **84**, 085312 (2011).

[26] E. J. König, P. M. Ostrovsky, I. V. Protopopov, I. V. Gornyi, I. S. Burmistrov, and A. D. Mirlin, Half-integer quantum Hall effect of disordered Dirac fermions at a topological insulator surface, Phys. Rev. B **90**, 165435 (2014).

[27] Y. Xu, I. Miotkowski, C. Liu, J. Tian, H. Nam, N. Alidoust, J. Hu, C. K. Shih, M. Z. Hasan and Y. P. Chen, Observation of topological surface state quantum Hall effect in an intrinsic three-dimensional topological insulator, Nat. Phys. **10**, 956 (2014).

[28] S. Zhang, L. Pi, R. Wang, G. Yu, X.-C. Pan, Z. Wei, J. Zhang, C. Xi, Z. Bai, F. Fei, M. Wang, J. Liao, Y. Li, X. Wang, F. Song, Y. Zhang, B. Wang, D. Xing, and G. Wang, Anomalous quantization trajectory and parity anomaly in Co cluster decorated BiSbTeSe$_2$ nanodevices, Nat. Commun. **8**, 977 (2017).

[29] J. Böttcher, C. Tutschku, L. W. Molenkamp, and E. M. Hankiewicz, Survival of the Quantum Anomalous Hall Effect in Orbital Magnetic Fields as a Consequence of the Parity Anomaly, Phys. Rev. Lett. **123**, 226602 (2019).

[30] M. Mogi, Y. Okamura, M. Kawamura, R. Yoshimi, K. Yasuda, A. Tsukazaki, K. S. Takahashi, T. Morimoto, N. Nagaosa, M. Kawasaki, Y. Takahashi, and Y. Tokura, Experimental signature of parity anomaly in semi-magnetic topological insulator, Nat. Phys. **18**, 390 (2022).

[31] D. J. Thouless, M. Kohmoto, M. P. Nightingale, and M. den Nijs, Quantized Hall Conductance in a Two-Dimensional Periodic Potential, Phys. Rev. Lett. **49**, 405 (1982).

[32] D. Xiao, M. C. Chang, and Q. Niu, Berry phase effects on electronic properties, Rev. Mod. Phys. **82**, 1959 (2010).

[33] B. Fu, J. Y. Zou, Z. A. Hu, H. W. Wang, and S. Q. Shen, Quantum anomalous semimetals, npj Quantum Mater. **7**, 94 (2022).

[34] J. Y. Zou, B. Fu, H. W. Wang, Z. A. Hu, and S. Q. Shen, Half-quantized Hall effect and power law decay

of edge-current distribution, Phys. Rev. B **105**, L201106 (2022).

[35] H. Zhang, C. X. Liu, X. L. Qi, X. Dai, Z. Fang, and S. C. Zhang, Topological insulators in Bi$_2$Se$_3$, Bi$_2$Te$_3$ and Sb$_2$Te$_3$ with a single Dirac cone on the surface, Nat. Phys. **5**, 438 (2009).

[36] Y. Xia, D. Qian, D. Hsieh, L. Wray, A. Pal, H. Lin, A. Bansil, D. Grauer, Y. S. Hor, R. J. Cava and M. Z. Hasan, Observation of a large-gap topological-insulator class with a single Dirac cone on the surface, Nat. Phys. **5**, 398 (2009).

[37] Y. L. Chen, J. G. Analytis, J.-H. Chu, Z. K. Liu, S.-K. Mo, X. L. Qi, H. J. Zhang, D. H. Lu, X. Dai, Z. Fang, S. C. Zhang, I. R. Fisher, Z. Hussan, and Z.-X. Shen, Experimental realization of a three-dimensional topological insulator, Science **325**, 178 (2009).

[38] R. Yu, W. Zhang, H. J. Zhang, S. C. Zhang, X. Dai, and Z. Fang, Quantized anomalous Hall effect in magnetic topological insulators, Science **329**, 61 (2010).

[39] Y. L. Chen, J. H. Chu, J. G. Analytis, Z. K. Liu, K. Igarashi, H. H. Kuo, X. L. Qi, S. K. Mo, R. G. Moore, D. H. Lu, M. Hashimoto, T. Sasagawa, S. C. Zhang, I. R. Fisher, Z. Hussain, and Z. X. Shen, Massive Dirac fermion on the surface of a magnetically doped topological insulator, Science **329**, 659 (2010).

[40] C. Z. Chang, J. Zhang, X. Feng, J. Shen, Z. Zhang, M. Guo, K. Li, Y. Ou, P. Wei, L. L. Wang, Z. Q. Ji, Y. Feng, S. Ji, X. Chen, J. Jia, X. Dai, Z. Fang, S. C. Zhang, K. He, Y. Wang *et al.*, Experimental observation of the quantum anomalous Hall effect in a magnetic topological insulator, Science **340**, 167 (2013).

[41] R. Yoshimi, K. Yasuda, A. Tsukazaki, K. S. Takahashi, N. Nagaosa, M. Kawasaki, and Y. Tokura, Quantum Hall states stabilized in semi-magnetic bilayers of topological insulators, Nat. Commun. **6**, 8530 (2015).

[42] C. X. Liu, X. L. Qi, H. J. Zhang, X. Dai, Z. Fang, and S. C. Zhang, Model Hamiltonian for topological insulators, Phys. Rev. B **82**, 045122 (2010).

[43] W. Y. Shan, H. Z. Lu, and S. Q. Shen, Effective continuous model for surface states and thin films of three-dimensional topological insulators, New J. Phys. **12**, 043048 (2010).

[44] H. Z. Lu, W. Y. Shan, W. Yao, and Q. Niu, and S. Q. Shen, Massive Dirac fermions and spin physics in an ultrathin film of topological insulator, Phys. Rev. B **81**, 115407 (2010).

[45] J. Linder, T. Yokoyama, and A. Sudbø, Anomalous finite size effects on surface states in the topological insulator Bi$_2$Se$_3$, Phys. Rev. B **80**, 205401 (2009).

[46] G. D. Mahan, *Many-Particle Physics* (Springer, New York, 2000).

[47] E. Prodan, Disordered topological insulators: A noncommutative geometry perspective, J. Phys. A: Math. Theor. **44**, 113001 (2011).

[48] C. W. J. Beenakker, Random-matrix theory of quantum transport, Rev. Mod. Phys. **69**, 731 (1997).

[49] C. W. Groth, M. Wimmer, A. R. Akhmerov, J. Tworzydło, and C. W. J. Beenakker, Theory of the Topological Anderson Insulator, Phys. Rev. Lett. **103**, 196805 (2009).

[50] R. B. Laughlin, Quantized Hall conductivity in two dimensions, Phys. Rev. B **23**, 5632 (1981).

[51] H. Haug and A.-P. Jauho, *Quantum Kinetics in Transport and Optics of Semiconductors* (Springer-Verlag, Berlin, 1996).